# Structure of the $Y_D$ Tyrosine Radical in Photosystem II as Revealed by $^2H$ Electron Spin Echo Envelope Modulation (ESEEM) Spectroscopic Analysis of Hydrogen Hyperfine Interactions[1]

**Kurt Warncke, Gerald T. Babcock, and John McCracken***

*Contribution from the Department of Chemistry, Michigan State University, East Lansing, Michigan 48824*

*Received April 4, 1994*®

**Abstract:** Electron spin echo envelope modulation (ESEEM) spectroscopic techniques have been used to characterize strong hydrogen hyperfine interactions in the $Y_D$ tyrosine radical in randomly oriented photosystem II reaction center protein isolated from *Synechocystis* 6803. Strains of *Synechocystis* rendered auxotrophic for aromatic amino acids were used to incorporate $^2H$-label at the 3,5-ring or methylene bridge positions of $Y_D^\bullet$ specifically. Stimulated echo envelope modulation was generated by conventional and pulse-swapping three-pulse sequences. Envelope-divided spectra of 3,5-$^2H$-/fully-protonated-$Y_D^\bullet$ obtained for $\tau$ values from 143 to 1388 ns (9.132 GHz, 0.3265 T) display distinctive $\tau$-suppression effects on the fundamental and double-quantum hyperfine frequencies. Simulations of the spectra yielded magnitudes and signs of the principal components of the total hyperfine tensor, [-3.0, -3.9, -1.1] MHz, and unpaired $p_\pi$ spin density at the 3,5-positions of 0.25 was estimated from the isotropic coupling. Multifrequency studies of the methylene-$^2H$-labeled $Y_D^\bullet$ displayed two pairs of hyperfine couplings that are assigned to two magnetically inequivalent $^2H$ nuclei. Simulations of the methylene-$^2H$ spectra give the following tensor values (axial dipolar tensor symmetry and signs assumed): $^2H_{\beta,2}$, [$A_\perp$ = 0.8, $A_\parallel$ = 2.2] MHz; $^2H_{\beta,1}$, [$A_\perp$ = 3.1, $A_\parallel$ = 4.5] MHz. Computations based on the standard description of $\beta$-hyperfine coupling, constrained by the relative spectral amplitudes and the two isotropic coupling constants, revealed dihedral angles between the planes of the ring-$C_1$—$C_\beta$—$^2H_\beta$ atoms and phenol ring of 52° and 68° and an unpaired $p_\pi$ spin density at $C_1$ of 0.37. There is no detectable static or dynamic dispersion in the dihedral angles from 4.2 to 77 K. The conformation of the methylene bridge is therefore fixed discretely by the protein. An independent estimation of the $C_1$ spin density of 0.36 was obtained from the common dipolar coupling strength (0.47 MHz) of $H_{\beta,1}$ and $H_{\beta,2}$ and the C1-to-$H_\beta$ distance in L-tyrosine crystals. This allows estimation of static values for the $^2H$ isotropic $\beta$-hyperfine coupling coefficients, $B_0$ and $B_2$, of $<|0.1|$ and 25.7 MHz, respectively. Comparison of the spin density distributions and dihedral angles among $Y_D^\bullet$ and model tyrosine neutral radicals in solution, crystalline, and glassy environments reveals factors contributing to the tyrosine radical energetics and redox potential of the couple and suggests an electronic mechanism for enhancement of directional selectivity in electron transfers mediated by tyrosine and other organic cofactor radicals.

## Introduction

The participation of amino acid-derived organic radicals in enzyme-mediated reactions is an emerging theme in biological catalysis. Organic radicals that are formed from posttranslationally modified tyrosine or tryptophan side chains[2] perform a dual role as centers for bond-making, bond-breaking chemistry and as electron-transfer cofactors. Radicals derived from unmodified tyrosine side chains appear to function as electron-transfer cofactors or hydrogen-transfer agents.[3,4] One of the first amino acid-based radicals to be identified,[5] the room temperature-stable tyrosine radical, $Y_D^\bullet$, is present in the photosystem II (PS II) reaction center (RC) protein of green plants and algae.[6,7] The function of the charge-neutral[8,9] $Y_D$ radical is not clear; the kinetics of its participation in intraprotein electron-transfer reactions appear to be too slow for an integral role in PS II turnover.[6] However, the electron paramagnetic resonance (EPR) spectrum of $Y_D^\bullet$ is similar to that of the $Y_Z$ tyrosine radical in the PS II RC protein, which functions as the metastable intermediate in electron transfer between the water-oxidizing manganese center

* Abstract published in *Advance ACS Abstracts*, July 1, 1994.
(1) This work is supported by the USDA Competitive Grants Office (G.T.B.) and NIH Grants GM-37300 (G.T.B.) and GM-45795 (J.M.).

(2) (a) Janes, S. M.; Mu, D.; Wemmer, D.; Smith, A. J.; Kaur, S.; Maltby, D.; Burlingame, A. L.; Klinman, J. P. *Science* **1990**, *248*, 981–987. (b) Dooley, D. M.; McGuirl, M. A.; Brown, D. E.; Turowski, P. N.; McIntire, W. S.; Knowles, P. F. *Nature* **1991**, *349*, 262–264. (c) Ito, N.; Phillips, S. E. V.; Steven, C.; Ogel, Z. B.; McPherson, M. J.; Keen, J. N.; Yadav, K. D. S.; Knowles, P. F. *Nature* **1991**, *350*, 87–90. (d) McIntire, W. S.; Wemmer, D. E.; Chistoserdov, A.; Lidstrom, M. E. *Science* **1991**, *252*, 817–824. (e) Davidson, V. L. *Principles and Applications of Quinoproteins*; Davidson, V. L., Ed.; Marcel Dekker: New York, 1992. (f) Babcock, G. T.; El-Deeb, M. K.; Sandusky, P. O.; Whittaker, M. M.; Whittaker, J. W. *J. Am. Chem. Soc.* **1992**, *114*, 3727–3734. (g) Warncke, K.; Babcock, G. T.; Dooley, D. M.; McGuirl, M. A.; McCracken, J. *J. Am. Chem. Soc.* **1994**, *116*, 4028–4037.

(3) (a) Ehrenberg, A.; Reichard, P. *J. Biol. Chem.* **1972**, *247*, 3485. (b) Sjöberg, B.-M.; Reichard, P.; Gräslund, A.; Ehrenberg, A. *J. Biol. Chem.* **1978**, *253*, 6863. (c) Prince, R. C. *Trends Biochem. Sci.* **1988**, *13*, 286–288. (d) Stubbe, J. *Annu. Rev. Biochem.* **1989**, *58*, 257–285. (e) Kolmacz, P. J.; Ren, Y.; Tsai, A.-L.; Palmer, G. *Biochemistry* **1990**, *29*, 8760–8771. (f) Smith, W. L.; Eling, T. E.; Kulmacz, R. J.; Marnett, L. J.; Tsai, A. L. *Biochemistry* **1992**, *31*, 3–7.

(4) Hoganson, C. W.; Babcock, G. T. *Biochemistry* **1992**, *31*, 11874–11880.

(5) (a) Barry, B. A.; Babcock, G. T. *Proc. Natl. Acad. Sci. U.S.A.* **1987**, *84*, 7099–7103. (b) Debus, R. J.; Barry, B. A.; Babcock, G. T.; McIntosh, L. *Proc. Natl. Acad. Sci. U.S.A.* **1988**, *85*, 427–430. (c) Debus, R. J.; Barry, B. A.; Sithole, I.; Babcock, G. T.; McIntosh, L. *Biochemistry* **1988**, *27*, 9071–9074. (d) Vermaas, W. F.; Rutherford, A. W.; Hannson, O. *Proc. Natl. Acad. Sci. U.S.A.* **1988**, *85*, 8477–8481. (e) Metz, J. G.; Nixon, P. J.; Roegner, M.; Brudvig, G. W.; Diner, B. A. *Biochemistry* **1989**, *28*, 6960–6969.

(6) Babcock, G. T.; Barry, B. A.; Debus, R. J.; Hoganson, C. W.; Atamian, M.; McIntosh, L.; Sithole, I.; Yocum, C. F. *Biochemistry* **1989**, *28*, 9557–9565.

(7) (a) Barry, B. A. *Photochem. Photobiol.* **1993**, *57*, 179–188. (b) Babcock, G. T. *Proc. Natl. Acad. Sci. U.S.A.* **1993**, *90*, 10893–108957. (c) Hoganson, C. W.; Babcock, G. T. In *Metal Ions in Biological Systems, Volume 30: Metalloenzymes Involving Amino-acid Residue and Related Radicals*; Sigel, H., Sigel, A., Eds.; Marcel Dekker: New York, 1994; pp 77–107.

(8) Barry, B. A.; Babcock, G. T. *Chem. Scripta* **1988**, *A28*, 117–122.

(9) Evelo, R. G.; Hoff, A. J.; Dikanov, S. A.; Tryshkin, A. M. *Chem. Phys. Lett.* **1989**, *161*, 479–484.

0002-7863/94/1516-7332$04.50/0 

**Chart 1**

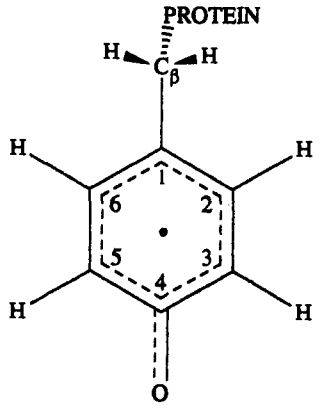


$Y_D$ tyrosine neutral radical (**1**)

and the photooxidized primary donor, $P680^{+}$.[6,10] The stability of $Y_D^{\bullet}$ makes it more amenable to spectroscopic examination than the fleeting $Y_Z$ radical. Characterization of the structure of $Y_D^{\bullet}$ in wild type PS II and in enzyme with site-directed mutations,[11] and comparison with the structures of model tyrosine radicals *in vitro*,[4,12-17] is vital for gaining insight into how protein promotes stability and specialized catalytic functions of tyrosine radicals *in situ*.

Details of the electronic and nuclear structure of $Y_D^{\bullet}$ (**1**) (Chart 1) can be revealed by the strength and symmetry of the hyperfine interactions between unpaired $\pi$-electron spin density ($\rho_\pi$) delocalized about the phenol ring and the $\alpha$-type 2,6- and 3,5- and $\beta$-type methylene-hydrogen nuclei.[18,19] The 2,6- and 3,5-hydrogen nuclei are essentially magnetically equivalent,[12-14] which facilitates study of the radicals by techniques of electron paramagnetic resonance (EPR) spectroscopy. A comprehensive simulation study of the EPR spectra of fully protonated $Y_D^{\bullet}$ in randomly oriented and oriented PS II RC protein in the solid state, and $Y_D^{\bullet}$ in randomly oriented RC protein in which distinct changes in the spectra were wrought by selective $^2H$-labeling at the 3,5- and methylene positions, has provided estimates or limits for the hyperfine tensors.[4] In order to specify accurately the tensor values and spin densities, however, hydrogen hyperfine couplings that are obscured by inhomogeneous broadening of the EPR spectrum must be resolved by monitoring directly the radiofrequency hyperfine transitions. An established technique is continuous-wave $^1H$ electron nuclear double-resonance spectroscopy (CW-ENDOR).[20] However, ENDOR has not been completely successful in measuring hyperfine couplings in $Y_D^{\bullet}$, in part because the detergent-solubilized, membrane protein samples are inherently paramagnetically dilute. In addition, the spin–spin interactions of the tyrosine radicals with nearby paramagnetic metal centers in ribonucleotide diphosphate reductase (RDPR) and prostaglandin H-synthase, which have dramatically enhanced ENDOR sensitivity in thorough studies of these radicals[21] (Shi, W.; Hoganson, C. W.; Espe, M.; Bender, C.; Tsai, A.-H.; Babcock, G. T. In preparation), are absent for $Y_D^{\bullet}$. In general, the large anisotropy of strong $\alpha$-hyperfine interactions causes a broad spectral extent, which can place portions of the transitions in regions of weak ENDOR enhancement and poor instrument sensitivity.[20a,22] The latter difficulty is also encountered for strong $\beta$-hydrogen couplings.

It has been demonstrated in systematic investigations of model tyrosine radicals that electron spin echo envelope modulation spectroscopy (ESEEM)[23] of $^2H$ nuclei is a powerful approach for the sensitive detection and detailed characterization of strong, anisotropic $\alpha$-hydrogen[16] and $\beta$-hydrogen[17] interactions. In the present work, we direct the stimulated echo ESEEM techniques developed in the model systems to the analysis of the 3,5-$^2H$ and methylene-$^2H$ hyperfine interactions in specifically labeled $Y_D^{\bullet}$ in the PS II RC protein isolated from tyrosine-auxotrophic strains of the blue-green algae *Synechocystis* 6803.[5a-c] The principal advantages of the $^2H$ ESEEM techniques for this analysis are as follows:[16,17] (a) The detection sensitivity of ESEEM is inherently high for low nuclear gyromagnetic ratio ($\gamma_N$) nuclei, such as $^2H$.[24,25] (b) The relatively low $\gamma_N$ of $^2H$ also leads to a concentration of anisotropically broadened hyperfine transitions in a relatively narrow spectral band and assures complete excitation[24] of the EPR transitions that access the $^2H$ hyperfine nuclear sublevels. (c) The narrow $^2H$ line widths eliminate undesired line-shape distortion arising from the ESE spectrometer dead time, because $(\Delta\nu_{line})^{-1} > \tau_{dead}$.[26] (d) The envelope modulation depth increases with the number of coupled nuclei,[24,25] and for strong modulation of long duration, harmonics of the fundamental frequencies provide additional constraints for determination of the number of magnetically equivalent or near-equivalent nuclei.[27] (e) The $^2H$ nucleus has a $\Delta m_I = \pm 2$, or "double quantum", transition that can provide additional spectral information.

The present analysis yields the principal components of the total 3,5- and methylene-hydrogen hyperfine tensors in $Y_D^{\bullet}$. From this information, values for $\rho_\pi$ at $C_1$, $C_3$, and $C_5$, and the conformations of the two methylene-hydrogen nuclei ($H_{\beta,1}$, $H_{\beta,2}$) relative to the phenol ring plane, are determined. From the measured spin densities, $\rho_\pi$ is estimated for $C_2$, $C_6$, and the combined $C_4$,O centers. Comparison with the hyperfine couplings in model tyrosine radicals suggests options open to protein for tailoring $Y_D^{\bullet}$, $Y_Z^{\bullet}$, and other tyrosine radicals for catalysis.

## Materials and Methods

**Preparation of Photosystem II RC Protein.** Aromatic amino acid auxotrophic strains of *Synechocystis* 6803 were grown and manipulated to incorporate $^2H$-labeled tyrosine as described.[15] Photosystem II particles were isolated as described.[28] Incorporation of the 3,5-$^2H$-tyrosine was

(10) Babcock, G. T. In *New Comprehensive Biochemistry 15: Photosynthesis*; Amez, J., Ed.; Elsevier North Holland: Amsterdam, 1987; pp 125–158.

(11) (a) Tang, X.-S.; Chisolm, D. A.; Dismukes, G. C.; Brudvig, G. W.; Diner, B. A. *Biochemistry* **1993**, *32*, 13742–13748. (b) Tommos, C.; Davidsson, L.; Svennson, B.; Madsen, C.; Vermaas, W.; Styring, S. *Biochemistry* **1993**, *32*, 5436–5441.

(12) Fasenella, E. L.; Gordy, W. *Proc. Natl. Acad. Sci. U.S.A.* **1969**, *62*, 299–304.

(13) Box, H. C.; Budzinski, E. E.; Freund, H. G. *J. Chem. Phys.* **1974**, *61*, 2222–2226.

(14) Sealy, R. C.; Harman, L.; West, P. R.; Mason, R. P. *J. Am. Chem. Soc.* **1985**, *107*, 3401–3406.

(15) Barry, B. A.; El-Deeb, M. K.; Sandusky, P. O.; Babcock, G. T. *J. Biol. Chem.* **1990**, *265*, 20139–20143.

(16) Warncke, K.; McCracken, J. *J. Chem. Phys.* **1994**, *101*, no. 3.

(17) Warncke, K.; McCracken, J. *J. Phys. Chem.*, submitted.

(18) (a) McConnell, H. M. *J. Chem. Phys.* **1958**, *28*, 107–117. (b) McConnell, H. M.; Strathdee. *J. Mol. Phys.* **1959**, *2*, 129–138. (c) Heller, C.; McConnell, H. M. *J. Chem. Phys.* **1960**, *32*, 1535–1539.

(19) (a) Carrington, A.; McLachlan, A. D. *Introduction to Magnetic Resonance*; Chapman and Hall: New York, 1980. (b) Gordy, W. In *Techniques of Chemistry, Volume XV: Theory and Applications of Electron Spin Resonance*; West, W., Ed.; Wiley & Sons: New York, 1980. (c) Wertz, J. E.; Bolton, J. R. *Electron Spin Resonance*; Chapman & Hall: New York, 1986.

(20) (a) Kevan, L.; Kispert, L. D. *Electron Spin Double Resonance Spectroscopy*; Wiley & Sons: New York, 1976. (b) Lubitz, W.; Babcock, G. T. *Trends Biochem. Sci.* **1987**, *12*, 96–100. (c) Bender, C. J.; Aisen, P. *Methods Enzymol.* **1993**, *227*, part D, 190–231.

(21) Bender, C. J.; Sahlin, M.; Babcock, G. T.; Barry, B. A.; Chandreshekar, T. K.; Salowe, S. P.; Stubbe, J.; Lindström, B.; Petersson, L.; Ehrenberg, A.; Sjöberg, B.-M. *J. Am. Chem. Soc.* **1989**, *111*, 8076–8083.

(22) Hyde, J. S.; Rist, G. H.; Eriksson, L. E. G. *J. Phys. Chem.* **1968**, *72*, 4269–4276.

(23) (a) Kevan, L.; Bowman, M. K. *Modern Pulsed and Continuous Wave Electron Spin Resonance*; John Wiley & Sons: New York, 1990. (b) Schweiger, A. *Angew. Chem., Int. Ed. Engl.* **1991**, *30*, 265–292.

(24) Rowan, L. G.; Hahn, E. L.; Mims, W. B. *Phys. Rev.* **1965**, *137*, A61–A71.

(25) Mims, W. B. *Phys. Rev. B* **1972**, *5*, 2409–2419.

(26) Astashkin, A. V.; Dikanov, S. A.; Tsvetkov, Yu. D. *Chem. Phys. Lett.* **1987**, *136*, 204–208.

(27) (a) Lin, C. P.; Bowman, M. K.; Norris, J. R. *J. Chem. Phys.* **1986**, *85*, 56–62. (b) McCracken, J.; Pember, S.; Benkovic, S. J.; Villafranca, J. J.; Miller, R. J.; Peisach, J. *J. Am. Chem. Soc.* **1988**, *110*, 1069–1074.

(28) Norin, G. H.; Boerner, R. J.; Barry, B. A. *Biochemistry* **1991**, *30*, 3943–3950.

stoichiometric, as shown by the characteristic EPR spectrum of the labeled $Y_D^{\bullet}$.[15] However, a prolonged growth period during labeling with the methylene-$^2$H tyrosine allowed some incorporation of the fully protonated tyrosine,[29] as shown by ENDOR measurements (Bowlby, N.; Espe, M.; Babcock, G. T. Unpublished) and the ESEEM results reported here. Comparison of the amplitudes of the strong-$^1$H methylene features that are observed in the partially-$^2$H-labeled and fully protonated samples (Warncke, K.; Babcock, G. T.; McCracken, J. Manuscript in preparation) suggests that approximately 40% of the $Y_D^{\bullet}$ observed incorporates $^2$H at the methylene positions. Fully protonated tyrosine and specifically labeled 3,5-$^2$H-tyrosine were obtained from Aldrich and Cambridge Isotope Laboratories, respectively.

**EPR Sample Preparation.** Photosystem II particles in 50 mM MES, 25% (v/v) glycerol, 0.05% (w/v) lauryl maltoside, 20 mM $CaCl_2$, and 15 mM NaCl buffer (pH = 6.0) were precipitated with an equal volume of 30% (w/v) polyethylene glycol (8000 g/mol) prior to loading into 4 mm o.d. EPR tubes. The samples were concentrated by pelleting in the EPR tubes by a brief centrifugation. Illumination with the off-center output of a 250-W projector lamp was performed for 1 min at 277 K. The samples were then dark-adapted on ice for 10–15 min before freezing for storage at 77 K. The CW-EPR spectra of the samples (110 K) were identical with those reported previously for samples prepared by this method.[15] The CW-EPR spectra were obtained at X-band on a Bruker ER200D EPR spectrometer outfitted with a Bruker TE102 EPR cavity. The external magnetic field strength was measured with a Bruker ER035M NMR gaussmeter, and the microwave frequency was measured with an EIP Microwave Model 25B frequency counter.

**ESEEM Spectroscopy.** The home-built pulsed-EPR spectrometer used in this work has been described.[30] Reconstruction of envelope modulation that was lost in the time interval $\tau + T_0$ in the three-pulse experiments was performed prior to Fourier transformation as described.[31]

**Theoretical Simulations.** Computer simulation of the ESEEM data was based on the density matrix treatment of Mims.[25,32] Simulations were run on a DEC Vaxstation 4000 or on Apple Macintosh II computers. The experimental dead time was included in the time domain simulations, with the dead time reconstruction[31] performed prior to Fourier transformation. This is the same method used in the analysis of the experimental data. Computations of the $\tau$-dependence of envelope modulation components were performed by using Matlab (Mathworks, Nantick, MA) programs on a Sun Sparcstation 2 or Macintosh II computers. Mutual random orientation for both the 3,5- and methylene-hydrogen nuclei was assumed in the simulations.

The success of the ESEEM simulations was judged according to the match with the experimental three-pulse ESEEM spectra on the basis of the following constraints: (a) the dependence of the line-shape widths and frequency positions of the intensity maxima and minima caused by $\tau$-suppression effects and (b) the magnetic field dependence of the line shapes and frequency positions at 0.3164, 0.3281, 0.3560, and 0.4056 T. Inclusion of the deuterium nuclear quadrupole interaction in the ESEEM simulations, by using typical values for the nuclear quadrupole coupling constant ($e^2qQ/4h$) of 0.05 MHz and electric field gradient asymmetry parameter ($\eta$) of 0.1,[33] did not alter significantly the spectra relative to those simulated in the absence of quadrupole coupling. This is because the quadrupole coupling is negligible in comparison with the strong hyperfine couplings considered in these studies.[16,17]

## Results

**3,5-$^2$H Hyperfine Interaction.** Figure 1 shows representative stimulated echo envelopes obtained by using the three-pulse, 90°–$\tau$–90°–$T$–90° microwave pulse sequence with pulse-swapping.[34] The collection of data for $T < 0$ that is made possible by the pulse-swapping sequence eliminates the long effective dead times associated with the large $\tau$ values that are necessary to resolve the full extent of the $^2$H ESEEM line shape.[16] As shown in

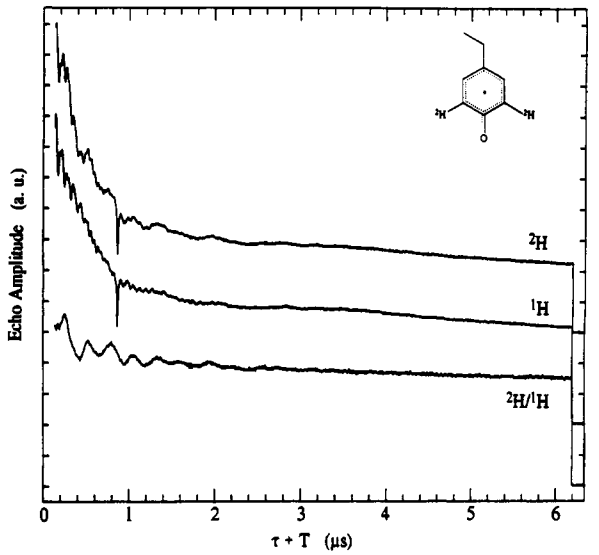


**Figure 1.** Stimulated echo envelope modulation generated by using the microwave pulse-swapping sequence. Time domains for the individual 3,5-$^2$H-$Y_D^{\bullet}$ and perprotonated $Y_D^{\bullet}$ and the quotient envelope are shown. Conditions are as follows: $\tau$, 855 ns; initial $T$ ($T_0$), –715 ns; initial $\tau + T_0$, 140 ns; microwave frequency, 9.185 GHz; magnetic field strength, 0.3293 T; microwave pulse power, 40 W (20 ns fWHM); pulse sequence repetition rate, 70 Hz; 10 events averaged per time point; temperature, 4.2 K.

Figure 1, both the discontinuity[35] and sharp spike in the individual wave forms that are caused by the eclipse of the second and third pulses are remedied by dividing the envelope modulation collected for the 3,5-$^2$H-labeled $Y_D^{\bullet}$ by the envelope for the fully protonated radical. As for envelope division applied in conventional two- and three-pulse experiments,[25,37] the contributions of $^2$H modulation in the quotient envelope are enhanced and modulation components from magnetic nuclei that are common to each radical are either eliminated or reduced significantly. In practice, modulation from strongly coupled $\alpha$-$^2$H is overwhelmingly dominant, so that contributions to the divided envelope from the 3,5-$^1$H nuclei replaced by $^2$H are not observed.[16]

Figure 2 shows ESEEM frequency spectra for the 3,5-$^2$H interaction in $Y_D^{\bullet}$ obtained by Fourier transformation of divided envelope modulation collected at different $\tau$ values. In each spectrum, intensity in the regions extending from approximately 0.5 to 1.5 and from 2.8 to 4.5 MHz arises from hyperfine splitting of the $m_s = +1/2$ (hyperfine frequency component, $\nu_\alpha$) and $m_s = -1/2$ ($\nu_\beta$) electron spin manifolds by interaction with the $^2$H nuclei.[38] The broad features reflect the anisotropy created by the orientation-dependence of the 3,5-$^2$H hyperfine frequencies together with the orientation-dependence of the ESEEM transition probabilities.[24,25] Combination features arising from the two equivalent $^2$H nuclei are not apparent, despite the strong modulation. This is attributed to the anisotropy of the couplings.[16] Weak combination features from the 3,5-$^2$H are discerned in tyrosine model radical studies at increased signal-to-noise ratios.[16]

(29) Bowlby, N. R.; Espe, M.; Bhatnagar, R.; Wang, J.; Hoganson, C.; McIntosh, L.; Babcock, G. T. *Photosynth. Res.* **1993**, *38*, 379–386.
(30) McCracken, J. L.; Shin, D.-H.; Dye, J. L. *Appl. Magn. Reson.* **1992**, *3*, 305–316.
(31) Mims, W. B. *J. Magn. Reson.* **1984**, *59*, 291–306.
(32) Mims, W. B. *Phys. Rev. B* **1972**, *6*, 3543–3545.
(33) Edmonds, D. T. *Phys. Lett. C* **1977**, *29*, 233–290.
(34) (a) Fauth, J. M.; Schweiger, A.; Braunschweiler, L.; Forrer, J.; Ernst, R. R. *J. Magn. Reson.* **1986**, *66*, 74–86. (b) Fauth, J. M.; Schweiger, A.; Ernst, R. R. *J. Magn. Reson.* **1989**, *81*, 262–274.

(35) At times $T < 0$ prior to pulse crossover, the envelope decay is dominated by relaxation processes that contribute to the phase memory time ($T_m$), and at times $T > 0$, by the longer spin–lattice relaxation time ($T_1$) processes. In glassy samples of model or protein-associated organic radicals present at concentrations of 0.05–0.3 mM, we typically encounter values of approximately 2–4 $\mu$s and >30 $\mu$s for $T_m$ and $T_1$, respectively, as reported elsewhere.[36] The following factors contribute to a glitch at pulse crossover: (a) the finite microwave pulse widths, (b) differences in the turn angles for the two- and three-pulse echoes, and (c) for limited data sampling, incomplete elimination of overlapping two-pulse echoes by the phase-cycling procedure.
(36) Brown, I. M. In *Time Domain Electron Spin Resonance*; Kevan, L., Schwartz, R., Eds.; Wiley and Sons: New York, 1979; pp 195–230.
(37) Mims, W. B.; Peisach, J. In *Advanced EPR: Applications in Biology and Biochemistry*; Hoff, A. J., Ed.; Elsevier: New York, 1989; pp 1–57.
(38) When the signs of the principal values, $A_i$, are negative, as is the case for $\alpha$-hydrogen hyperfine interactions, the lower frequency fundamental feature corresponds to $\nu_\alpha$ and the higher frequency fundamental to $\nu_\beta$. When the signs of $A_i$ are positive, as is the case for $\beta$-hydrogen hyperfine interactions, the lower frequency fundamental feature corresponds to $\nu_\beta$ and the higher frequency fundamental to $\nu_\alpha$.

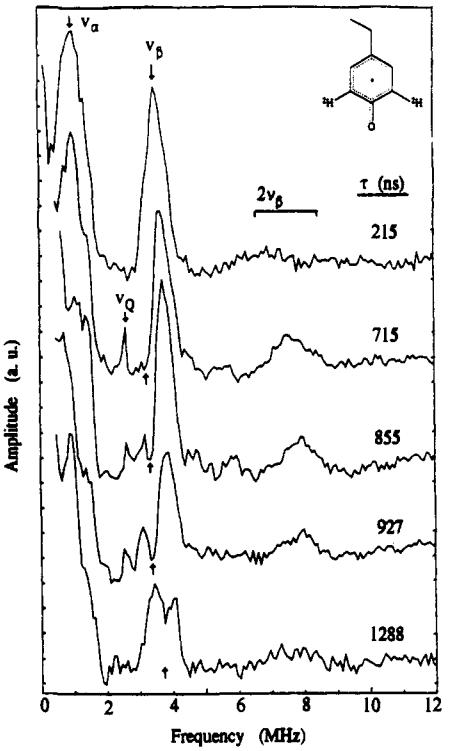


**Figure 2.** ESEEM spectra of the $Y_D$ radical from stimulated echo, 3,5-$^2H/^1H$ quotient envelope modulation collected at different values of $\tau$. Features corresponding to the $\nu_\alpha$, $\nu_\beta$, and $2\nu_\beta$ hyperfine frequencies are indicated. The feature denoted $\nu_Q$ arises from $^{14}N$ nuclear quadrupole coupling in contaminant chlorophyll radicals. Conditions are as follows: initial $\tau + T_0$, 140 ns; microwave frequency, 9.185 GHz; magnetic field strength, 0.3293 T; microwave pulse power, 40 W (20 ns fWHM); pulse sequence repetition rate, 70 Hz; 10 events averaged per time point; temperature, 4.2 K. The $\tau$ values chosen in these studies correspond to integral multiples of the reciprocal of the free proton frequency ($\nu_N^{-1}$ = 72 ns) in order to suppress the undesired contribution of matrix protons to the spectra.[32,37] The up-turned arrows indicate the minima of the $\tau$-suppression in the $\nu_\beta$ feature.

Differences among the line shapes of the spectra in Figure 2 are caused by the $\tau$-dependent suppression effect.[32] The suppression effect arises because the contributions of the $\nu_\alpha$ and $\nu_\beta$ frequencies to the echo envelope are governed in a $\tau$-dependent manner by the conjugate $\nu_\beta$ and $\nu_\alpha$ frequencies, respectively. When $\tau$ is chosen equal to one precession cycle of one frequency, say $\nu_\alpha$, the contribution of the conjugate frequency component, $\nu_\beta$, to the envelope modulation is suppressed, and "blind spots" are created in the line shapes.[32,37] At $\tau$ equal to half-integral values of $(\nu_\alpha)^{-1}$, the envelope modulation due to conjugate $\nu_\beta$ components is relatively enhanced. Systematic effects of $\tau$-suppression on the line shape are observed clearly in Figure 2 in the higher frequency, $\nu_\beta$, feature at $\tau$ values of 855, 927, and 1288 ns. The suppression minimum, which is marked by the up-turned arrows in Figure 2, tracks across the $\nu_\beta$ feature to higher frequency as the increase in $\tau$ actuates suppression from lower frequency conjugate $\nu_\alpha$ components. In addition, the depth of suppression exhibits an asymmetric dependence on position in the $\nu_\beta$ line, showing a nearly full effect on the low-frequency side and becoming less pronounced toward the high-frequency edge. Observation of this behavior in the lower frequency, $\nu_\alpha$ fundamental is partially obscured by an artifactual increase in the base line owing to a slight mismatch of the phase memory decay times ($T_m$) of the 3,5-$^2H$ and -$^1H$ samples.

In contrast to the strong intensity at the fundamental frequencies that is observed at all $\tau$ values, the spectra in Figure 2 show that maximum intensity at the $2\nu_\beta$, double-quantum frequencies is only manifest at relatively long values of $\tau$. Intensity emerges at short $\tau$ in the low-frequency portion of the double-quantum line. Increasing $\tau$ shifts the maximum frequency to higher values.

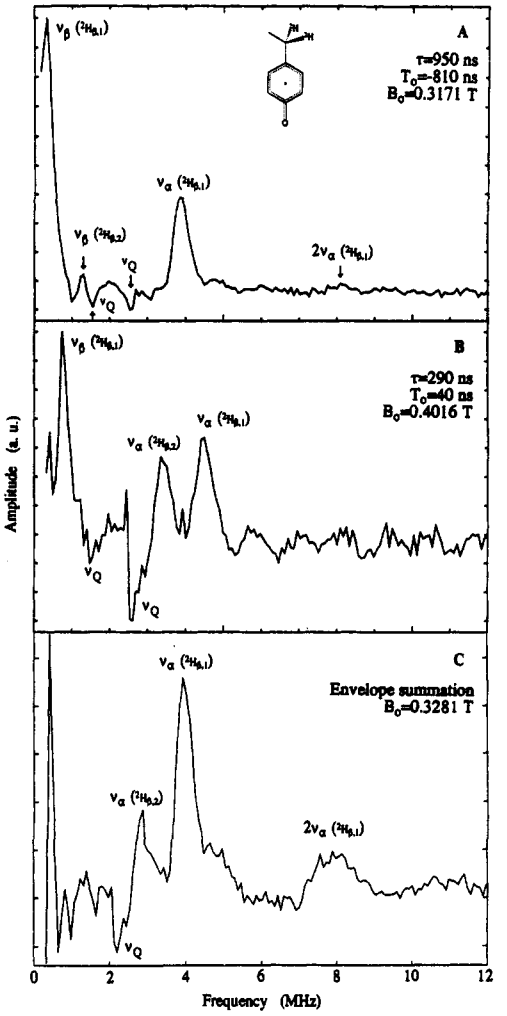


**Figure 3.** ESEEM spectra of the $Y_D$ radical from stimulated echo, methylene-$^2H/^1H$ quotient envelope modulation collected at different values of $\tau$. Features from the fundamental and double-quantum hyperfine frequencies for the weakly and strongly coupled methylene-$^2H$ nuclei are indicated. Contributions from $^{14}N$ nuclear quadrupole coupling in contaminant chlorophyll radicals are denoted by $\nu_Q$. (A) Spectrum from envelope modulation collected using the pulse swapping sequence. Conditions are as follows: $\tau$, 950 ns; initial $\tau + T_0$, 140 ns; microwave frequency, 8.820 GHz; magnetic field strength, 0.3171 T; microwave pulse power, 40 W (20 ns fWHM); pulse sequence repetition rate, 70 Hz; 30 events averaged per time point; temperature, 4.2 K. (B) Spectrum from envelope modulation collected using the conventional three-pulse sequence. Conditions are as follows: $\tau$, 290 ns; $T_0$, 40 ns; microwave frequency, 11.306 GHz; magnetic field strength, 0.4016 T; microwave pulse power, 40 W (20 ns fWHM); pulse sequence repetition rate, 70 Hz; 30 events averaged per time point; temperature, 4.2 K. (C) Spectrum from the methylene-$^2H/^1H$ quotient envelope obtained by summation of quotient envelopes obtained at the following $\tau$ values: 215, 286, 358, 429, 501, 573, 644, 716, 787, 859, 931, 1002, 1145, and 1288 ns. Conditions are as follows: initial $\tau + T_0$, 140 ns; microwave frequency, 9.134 GHz; magnetic field strength, 0.3281 T; microwave pulse power, 40 W (20 ns fWHM); pulse sequence repetition rate, 30 Hz; 10 events averaged per time point; temperature, 4.2 K.

This characteristic behavior can be explained in terms of the conjugate $\nu_\alpha$ suppression effects[32] on the $2\nu_\beta$ intensity.[16] The extents of the line-shape and the $\tau$-suppression behavior provide key constraints for simulations that are necessary to determine the 3,5-$^2H$ hyperfine tensor.

**Methylene-$^2H$ Hyperfine Interactions.** Figure 3 shows ESEEM frequency spectra obtained by Fourier transformation of the divided envelope modulation collected from methylene-$^2H$-labeled and fully protonated $Y_D^\bullet$. Figure 3A shows the spectrum from data collected at a magnetic field strength ($B_0$) of 0.3164 T by using the pulse-swapping sequence. Two dominant, positive features at 0.4 and 4.0 MHz are displaced roughly symmetrically

about the free precession frequency of $^2H$ ($\nu_N$). These low- and high-frequency features are assigned to the $\nu_\beta$ and $\nu_\alpha$ frequencies, respectively, of one methylene-$^2H$ nucleus.[38] This interaction is comparable in strength with a strong $^1H$ hyperfine coupling of 22.4 MHz in $Y_D^•$ from *Synechocystis*[4] assigned to a methylene-$^1H$, but is smaller than the coupling of 27.2 MHz attributed to an analogous interaction in $Y_D^•$ from spinach.[39]

Additional $^2H$ features are difficult to identify with certainty in the spectrum in Figure 3A. This is because the methylene-$^2H$ interaction is dominated by the isotropic coupling, which leads to decreased modulation depths relative to the strong modulation from the 3,5-$^2H$ nuclei in the 3,5-$^2H$-tyrosine-labeled PS II samples, where deep modulation is promoted by the simultaneous presence of strong dipolar and contact interactions.[25] The detection sensitivity is diminished further by the substoichiometric incorporation of $^2H$ at the methylene positions of $Y_D$ (see the Materials and Methods section). The spectra in Figure 3 therefore display prominently interference from other modulation sources. Chief among these is modulation at the nuclear quadrupole frequencies of pyrrole $^{14}N$ nuclei in chlorophyll radicals.[40] Despite the low concentrations of these undesired species, strong modulation is observed because the $^{14}N$ are near the condition of exact cancellation.[41] Contributions from these species centered at 1.5–1.6 and 2.6 MHz are noted as $\nu_Q$ in Figure 3. The 2.6-MHz feature is also observed in the 3,5-$^2H$-$Y_D^•$ spectra in Figure 2. In addition, there are low-frequency features arising from the $\nu_\beta$ features of the strong methylene-$^1H$ nucleus[39] (Warncke, K.; Babcock, G. T.; McCracken, J. Manuscript in preparation), which achieve maximum amplitude at $B_0 \sim 0.3200$ T.

The undesired modulation can be attenuated relative to the methylene-$^2H$ signals by performing experiments at higher $B_0$ values. The spectra presented in Figure 3B were obtained at $B_0 = 0.4016$ T by using the multifrequency capability of the ESE spectrometer. The $^2H$ line shape is moved *en bloc* by 0.5 MHz to higher frequency and thus beyond the congested low-frequency region. In contrast, the frequency positions of the $^{14}N$ nuclear quadrupole features are not sensitive to changes in magnetic field to first order, and the strong methylene-$^1H$ features are translated to >5 MHz and reduced to undetectable intensity (Warncke, K.; Babcock, G. T.; McCracken, J. Manuscript in preparation).

The spectrum in Figure 3B reveals a positive feature at 3.4 MHz that we assign to the $\nu_\alpha$ frequency of the second methylene-$^2H$ in $Y_D^•$. This weak methylene-hydrogen hyperfine coupling has previously eluded detection by EPR and CW-ENDOR spectroscopies.[4] In ESEEM spectra obtained at $B_0 \sim 0.3200$ T, this feature would be obscured by the $^{14}N$ feature at ~2.6 MHz, which accounts in part for its absence from the spectrum in Figure 3A. In Figure 3B, negligible intensity for the conjugate $\nu_\beta$ feature is observed in the region of 1.6–1.8 MHz because the $\tau$ value of 290 ns, chosen to suppress the matrix $^1H$ modulation,[37] is near to the value of $\nu_\alpha^{-1} = 294$ ns. This results in a complete suppression of $\nu_\beta$. In contrast, the $\tau$ value of 290 ns corresponds to complete enhancement of the 3.4-MHz $\nu_\alpha$ feature. Although we have observed intensity from the weak methylene-$^2H$ $\nu_\beta$ feature at other $\tau$ values, this coupling is generally obscured by the overlapping $^{14}N$ nuclear quadrupole lines. This feature is perceptible at 1.2 MHz in the spectrum shown in Figure 3A.

Figure 3C shows the spectrum obtained by Fourier transformation of the summation of envelope modulation collected by using the microwave pulse-swapping sequence at fourteen $\tau$ values at 72-ns intervals from 215 to 1288 ns at $B_0 = 0.3281$ T. In the spectrum of the envelope summation, the suppression effects on the line shape are attenuated, thus revealing the full extent of the ESEEM line shape determined primarily by the orientation-dependence of the ESEEM transition probabilities.[16,17,42] The summation spectrum shows the $\nu_\alpha$ feature of the strong methylene-$^2H$ hyperfine coupling and a feature extending from 7 to 9 MHz, which we assign to the double-quantum frequencies, $2\nu_\alpha$. The $2\nu_\alpha$ feature is also observed in individual spectra obtained by using the pulse-swapping sequence at long $\tau$ values (>500 ns). The amplitude of the double-quantum feature depends critically on the magnitude of the dipolar interaction and places exacting constraints on the dipolar coupling strength used in spectral simulations.

## Discussion

**1. 3,5-$^2H$ Hyperfine Interaction. Determination of the Hyperfine Tensor.** Simulation of the three-pulse $^2H$ ESEEM spectra has been performed in order to determine the 3,5-$^2H$ hyperfine tensor for the $Y_D$ radical. A representative simulation is presented in Figure 4A that corresponds to the experimental spectrum acquired at $\tau = 855$ ns. The principal values of the hyperfine tensor are listed in Table 1. The axes for the tensor are chosen such that the $x$- and $z$-directions correspond approximately to the $p_\pi$-orbital axis and C—H bond, respectively, with $y$ perpendicular to $z$ and in the ring plane. The hyperfine tensor may be rotated by up to 10° in the ring plane away from the molecular $y$- and $z$-axes, however, owing to weak dipolar interactions with near-neighbor spin density centers.[4,21,44] The unique correspondence between the rhombic hyperfine tensor and the appearance of the hyperfine frequencies in the stimulated echo ESEEM spectrum is conferred predominantly by the $\tau$-suppression effect.[16]

The hyperfine frequency dependence of partial suppression can be used to determine the relative sign of the isotropic component of strong $\alpha$-hydrogen hyperfine interactions when $|A_{iso}| \geq |2A_{dip,y}|$.[16] The degree of partial suppression decreases in the $x$, $y$ (axial) region of the line shape.[16] Figure 2 shows that the $x$-, $y$-region is on the high-frequency side of the $\nu_\beta$ line shape. Therefore, the isotropic coupling is negative in sign, as expected for an $\alpha$-hydrogen coupling.[19] Thus, the value of the isotropic coupling ($A_{iso}$) for $^2H$ ($^1H$) is −2.7 (−17.4) MHz. The magnitude of the isotropic coupling for the 2,6-$^2H$ hyperfine interactions can be estimated by using the following empirical relation: $|A_{iso}(3,5\text{-}^2H) + A_{iso}(2,6\text{-}^2H)| = 2.03 \pm 0.03$ MHz.[45] An $A_{iso}$ value for the 2,6-$^2H$ ($^1H$) hyperfine interaction of 0.67 (4.4) MHz is thus estimated. This $A_{iso}$ value is consistent with the principal values of the 2,6-$^1H$ hyperfine tensor in $Y_D^•$ determined by ENDOR studies, [|4.8|, |7.6|, |<2.2|] MHz.[46]

**Unpaired Spin Density at the 3,5-Positions.** An unpaired $p_\pi$-spin density at $C_3$ and $C_5$ of 0.25 is estimated by using a McConnell $Q_{CH}^H(^2H)$ value of −10.7 MHz.[21] A small magnitude, negative unpaired spin density of −0.06 is estimated at $C_2$, $C_6$. The $\rho_\pi$ at $C_3$, $C_5$ is lower than the value of 0.29 estimated from the simulation study of the $Y_D^•$ EPR spectra.[4] The value of $\rho_\pi = 0.25$ in $Y_D^•$ is the same as $\rho_\pi$ at $C_3$, $C_5$ calculated for model tyrosine neutral radicals present in L-tyrosine crystals (0.25)[12] and in low-temperature glass (0.25).[16] By using the reported $Q_{CH}^H$ value,[21]

(39) Evelo, R. G.; Dikanov, S. A.; Hoff, A. J. *Chem. Phys. Lett.* **1989**, *157*, 25–30.

(40) (a) Bowman, M. K.; Norris, J. R.; Thurnauer, M. C.; Warden, J.; Dikanov, S. A.; Tsvetkov, Yu. D. *Chem. Phys. Lett.* **1978**, *55*, 570–574. (b) Dikanov, S. A.; Tsvetkov, Yu. D.; Bowman, M. K.; Astashkin, A. V. *Chem. Phys. Lett.* **1982**, *90*, 149–153. (c) Dikanov, S. A.; Astashkin, A. V.; Tsvetkov, Yu. D.; Goldfeld, M. G. *Chem. Phys. Lett.* **1983**, *101*, 206–209. (d) Hoff, A. J.; De Groot, A.; Dikanov, S. A.; Astashkin, A. V.; Tsvetkov, Yu. D. *Chem. Phys. Lett.* **1985**, *118*, 40–47.

(41) (a) Mims, W. B.; Peisach, J. *J. Chem. Phys.* **1978**, *69*, 4921–4930. (b) Flanagan, H. L.; Singel, D. J. *J. Chem. Phys.* **1987**, *87*, 5606–5616. (c) Lai, A.; Flanagan, H. L.; Singel, D. J. *J. Chem. Phys.* **1988**, *89*, 7161–7166.

(42) The summation of spectra taken at different $\tau$ values in conventional three-pulse experiments has been suggested.[43] The use of pulse-swapping allows summation of time domain data acquired at different $\tau$ values, owing to the common data collection start point, which has the following advantages over the spectrum summation method:[16] (a) It is necessary to compute only one Fourier transform, (b) the spectrum is not subject to accumulated distortion from individual spectra collected at different $\tau$ values and, hence, different effective dead times, and (c) a minimum, instrumentation-limited dead time can be used.

(43) Merks, R. P. J.; DeBeer, R. *J. Magn. Reson.* **1980**, *37*, 305–319.

(44) O'Malley, P. J.; Babcock, G. T. *J. Am. Chem. Soc.* **1986**, *108*, 3995–4001.

(45) Dixon, W. T.; Moghimi, M.; Murphy, D. *J. Chem. Soc., Faraday Trans. 2* **1974**, *70*, 1713–1720.

(46) Espe, M. Doctoral Dissertation, Michigan State University, 1994.

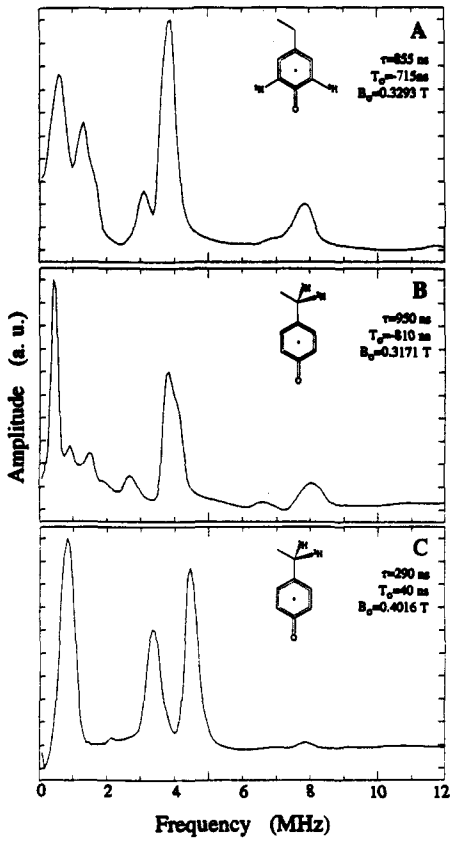


**Figure 4.** Simulations of ESEEM spectra for the 3,5-$^2H$ and methylene-$^2H$ hyperfine couplings in the $Y_D$ radical. All simulations incorporate the hyperfine tensor components presented in Table 1 and parameters corresponding to the conditions in Figures 2 and 3. The contributions of the $\nu_\alpha$, $\nu_\beta$, $2\nu_\alpha$, and $2\nu_\beta$ hyperfine frequencies in the spectra are indicated. (A) 3,5-$^2H$ interaction. Parameters are as follows: $\tau$ = 855 ns; $T_0$, −715 ns; $K$, 0.05 MHz; $\eta$, 0.1; magnetic field strength, 0.3293 T; two identical coupled $^2H$ are combined. (B) Methylene-$^2H$ interaction. Parameters are as follows: $\tau$, 950 ns; $T_0$, −810 ns; magnetic field strength, 0.3171 T; $K$, 0.05 MHz; $\eta$, 0.1. (C) Methylene-$^2H$ interaction. Parameters are as follows: $\tau$, 290 ns; $T_0$, 40 ns; magnetic field strength, 0.4016 T; $K$, 0.05 MHz; $\eta$, 0.1.

$\rho_\pi$ values at $C_3$, $C_5$ in the tyrosine neutral radical in solution at 296 K are estimated to be 0.25 from the $A_{iso}$ value determined previously.[14] These $\rho_\pi$ values are also within ±0.02 of values in other enzyme-bound tyrosine radicals.[4,21] The spin density at the phenol ring 3,5- and 2,6-positions is thus impervious to the influence of the different solvating environments of the tyrosine neutral radical, as concluded earlier.[4,15]

**Total Dipolar Interaction.** The dipolar components of the 3,5-$^2H$ hyperfine tensor represent the total dipolar interactions with unpaired spin density delocalized over $Y_D$•. The dipolar part of the $^2H$ hyperfine tensor, [−0.3, −1.2, +1.6] MHz, agrees within the uncertainty of the analysis with values for the total $^2H$ dipolar tensor determined in the model tyrosine neutral radical in rigid glass.[16] Therefore, the combination of the dominant dipolar interaction with the unpaired spin density at $C_3$, $C_5$ ($R$ = 1.09 Å)[47] and perturbations from dipolar fields emanating from neighbor nuclei ($R$ > 2.1 Å) are similar in these radicals. This suggests a comparable distribution of unpaired spin density in the solid-state model and $Y_D$ tyrosine radicals.

**2. Methylene-$^2H$ Hyperfine Interactions, Determination of the Two $^2H$ Hyperfine Tensors.** Theoretical simulations of the ESEEM spectra from methylene-$^2H$-labeled $Y_D$ radical, including data collected at $\tau$ values from 143 to 1288 ns and $B_0$ over a range 0.3164–0.4056 T, have been performed in order to determine the two hyperfine tensors. Figure 4B,C shows representative simulations, incorporating two coupled $^2H$ nuclei, combined in accord with the product rule.[24,25] Table 1 lists the hyperfine coupling values used in the simulations. The simulations correspond to the experimental spectra presented in Figure 3A,B. The requirement for two tensors is in agreement with the known structure of the $^2H$-methylene-labeled radical **1**. A dipolar hyperfine tensor of axial symmetry was assumed in the simulations, where $A_{dip,x} = A_{dip,y} = A_{dip,\perp} = -A_{dip}$ and $A_{dip,z} = A_{dip,\parallel} = 2A_{dip}$. Axial symmetry is supported by the small rhombicity ($|(A_{dip,x} - A_{dip,y})/A_{dip,z}|$) for the weakly-coupled methylene-$^1H$ nucleus in ribonucleotide diphosphate reductase of 0.095[21] and comparable rhombicities for conformationally restricted $\beta$-methyl-$^1H$ observed in single-crystal EPR studies.[19b] In addition, these small rhombicities predict a difference of ~|0.06| MHz between the $A_x$ and $A_y$ components for the methylene-$^2H$ hyperfine interaction in $Y_D$•, which would be difficult to resolve in the ESEEM experiments. This is because of the absence of distinct suppression incisions in the experimental line shapes does not permit the attribution of tensor rhombicity from suppression effects, as is the case for the broader 3,5-$^2H$ line shapes. The full width of the suppression at half-height under these conditions (~0.5 MHz, as gauged from the 3,5-$^2H$ spectra) is comparable with the line widths of the methylene-$^2H$ $\nu_\alpha$ and $\nu_\beta$ features.

The experimental spectrum in Figure 3A and corresponding simulated spectrum in Figure 4B are dominated by the features from the strongly coupled $^2H_\beta$ nucleus. This is because the magnitudes of the isotropic hyperfine and nuclear Zeeman interactions in the $\nu_\beta$ electron spin manifold approach equivalence, the "exact cancellation" condition which leads to a large enhancement of the modulation depth.[41] This condition is reflected in the spectra by the positioning of the $\nu_\beta$ feature near to the zero frequency. When the ESEEM measurements are performed at higher magnetic field (0.4016 T), the difference between the Zeeman and hyperfine contributions in the $\nu_\beta$ manifold is increased, as reflected in the shift of the maximum of the $\nu_\beta$ feature to 0.8 MHz, and the modulation depth for the strongly coupled $^2H_\beta$ nucleus is diminished from that at ~0.3200 T. This allows detection of ESEEM from the weakly coupled $^2H_\beta$ nucleus, as observed in Figure 3B and predicted in Figure 4C.

**Dihedral Angles and Unpaired Spin Density at $C_1$ Estimated from the Isotropic Coupling.** The unpaired spin density at $C_1$ and the dihedral angle, $\theta$, between the $C_1$—$C_\beta$—$H_\beta$ and phenol ring planes can be estimated from expressions that relate these parameters to the isotropic component of the $\beta$-hyperfine interaction.[18c] The geometry of the interaction is depicted in Figure 5. The expression takes the following form,[18c,19]

$$A_{iso} = \rho_\pi Q_\beta(\theta) \quad (1)$$

where $Q_\beta(\theta) = (B_0 + B_2 \cos^2\theta)$. The physical significance of $B_0$ is poorly understood.[19b,48] Reported experimental and theoretical $B_0$ values are generally 4–7% of $B_2$. Therefore, $B_0$ is commonly neglected in practical applications of eq 1, leading to the following expression:

$$A_{iso} \approx \rho_\pi(B_2 \cos^2\theta) \quad (2)$$

The coefficient $B_2$ represents the isotropic coupling resulting from the maximum exchange of unpaired spin density with $H_\beta$ through hyperconjugation of the $C_1$ $p_\pi$-orbital and $C_\beta$ p-orbital component involved in the $C_\beta$—$H_\beta$ $\sigma$-bonding orbital. Maximum hyperconjugative coupling occurs when the dihedral angle between $C_1$—$C_\beta$—$H_\beta$ and the $p_\pi$-orbital is 0°. As $\theta$ increases and the component of the $C_\beta$—$H_\beta$ bonding orbital along the $p_\pi$-orbital axis is decreased, the degree of hyperconjugative coupling, and hence isotropic interaction, decreases as $\cos^2\theta$. In the calculations, a value of $B_2$ for $^2H$ ($^1H$) of 24.9 MHz (162 MHz) is assumed,

(47) Frey, M. N.; Koetzle, T. F.; Lehmann, M. S.; Hamilton, W. C. *J. Chem. Phys.* **1973**, *58*, 2547–2556.

(48) (a) Colpa, J. P.; de Boer, E. *Mol. Phys.* **1964**, *7*, 333. (b) Morton, J. R. *Chem. Rev.* **1964**, *64*, 453–471. (c) Adam, F. C.; King, F. W. *J. Chem. Phys.* **1973**, *58*, 2446–2453.

**Table 1.** Principal Hyperfine Tensor Components and Isotropic Coupling Constants for the 3,5- and Methylene-Hydrogen Interactions with Unpaired Spin Density in the $Y_D$ Tyrosine Radical[a]

| assignment | $A_x$ | $A_y$ | $A_z$ | $A_{iso}$ | $\rho$ | $\theta$ |
|---|---|---|---|---|---|---|
| 3,5-H | −3.0 (−19.5) | −3.9 (−25.4) | −1.1 (−7.2) | −2.7 (−17.4) | 0.25 | |
| methylene-$H_{\beta,2}$ | 0.8 (5.2) | 0.8 (5.2) | 2.2 (14.3) | 1.27 (8.3) | 0.37 | 68° |
| methylene-$H_{\beta,1}$ | 3.1 (20.2) | 3.1 (20.2) | 4.5 (29.3) | 3.55 (23.1) | 0.37 | 52° |

[a] Assignment of the signs of the tensor components are described in the text. The values for $^2H$ ($^1H$) are given in units of MHz.

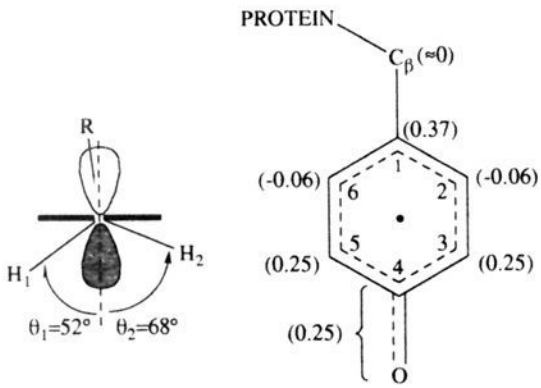


**Figure 5.** Structure of the $Y_D$ tyrosine radical in the PS II RC protein from *Synechocystis*: (left) conformation of the methylene-hydrogen atoms relative to the plane of the ring; the view is down the $C_1$—$C_\beta$ axis; (right) depiction of the spin densities at positions on the phenol side chain.

which was estimated from the isotropic coupling of freely rotating $\beta$-methyl-$^1H$ in aliphatic radicals in solution.[49] We also assume that the difference between the dihedral angles for the strongly ($\theta_1$) and weakly ($\theta_2$) coupled $\beta$-$^2H$ nuclei is $|120°|$, as expected for $sp^3$-hybridized $C_\beta$.[12,47] The measured isotropic hyperfine couplings of the two methylene-$^2H$ interactions then provide the constraints on eq 2 necessary to determine values of $\theta_1 = 52°$, $\theta_2 = 68°$, and $\rho_\pi = 0.37$ at $C_1$. These values are included in Table 1. Small unpaired s-spin densities of $|0.016|$ and $|0.002|$ at $^2H_{\beta,1}$ and $^2H_{\beta,2}$, respectively, are estimated by using the electron–proton coupling of 1420 MHz in the hydrogen atom.[19c] The $C_1$—$C_\beta$ conformation and spin densities around the phenol ring of $Y_D^\bullet$ are depicted in Figure 5.

The values for $\theta_1$ and $\theta_2$ in $Y_D^\bullet$ are close to the values of $\theta \approx 60°$ predicted to be thermodynamically most stable for each methylene-hydrogen from solution studies,[14] as well as by molecular mechanical modeling considerations. Therefore, the internal torsion potential energy of the $C_1$—$C_\beta$ bond is near a minimum, and the ring–$C_\beta$ link is essentially relaxed conformationally.

The $\rho_\pi$ value of 0.37 for $C_1$ lies in the upper range estimated for $Y_D^\bullet$ by EPR spectral simulations.[4] In comparison, $\rho_\pi$ values at $C_1$ of 0.32 and $0.34 \pm 0.02$ have been calculated for the tyrosine neutral radical in L-tyrosine crystals[12] and in low-temperature glasses,[17] respectively. Therefore, the values of $\rho_\pi$ at $C_1$ are comparable in $Y_D^\bullet$ and the model radicals in the solid state.

**Unpaired Spin Density at $C_1$ Estimated from the Dipolar Coupling.** The unpaired spin density at $C_1$ can be estimated independently from the strength of the $C_1$—$^2H_\beta$ dipolar hyperfine interaction. As required for this analysis, the line-broadening mechanism is hyperfine anisotropy, rather than spectral diffusion or other factors[50] that contribute to irreversible loss of phase coherence during and following the microwave pulses. This is shown by the amplitude of the $^2H_{\beta,1}$ double-quantum feature observed in the pulse-swapped spectra of Figure 3C, which requires absolutely the observed dipolar-coupling strength. In addition, narrower lines, with widths at half-maximum amplitude of 0.28 and 0.20 MHz, are observed at the matrix $^1H$ and $^{14}N$ nuclear quadrupole frequencies, respectively, in individual spectra. The comparable $\nu_\alpha$ line widths for each methylene-$^2H$ interaction show that differential coupling of $^2H_{\beta,1}$ and $^2H_{\beta,2}$ with dipolar fields emanating from neighbor ring nuclei is negligible, as expected from the amount of unpaired spin density at the ring carbon positions and separation distances of >4 Å.[47] In addition, the comparable dipolar interactions for $^2H_{\beta,1}$ and $^2H_{\beta,2}$ support the validity of the point dipole approximation and the simple physical model presented in Figure 5.

The spin density at $C_1$ is estimated in the point dipole limit by using values for the $C_1$—$H_\beta$ distance of $R = 2.1$ Å from neutron diffraction studies of diamagnetic tyrosine in crystals[47] and the dipolar-coupling constant, $A_{dip} = 0.47$ MHz, found from simulations of the experimentally indistinguishable line widths of the $^2H_{\beta,1}$ and $^2H_{\beta,2}$ $\nu_\alpha$ features by using the following expression:[19]

$$A_{dip} = g_e g_N \beta_e \beta_N \rho_\pi R^{-3} = 12.0 \rho_\pi R^{-3} \qquad (3)$$

A spin density at $C_1$ of 0.36 is estimated by using eq 3. This value is in good agreement with the value estimated from the isotropic coupling. The comparable $C_1$ spin densities calculated from the isotropic and dipolar interactions show that the model for the nuclear geometry (Figure 5) and the electronic models for hyperconjugation-mediated isotropic coupling are consistent. The agreement also indicates negligible contributions to the $\beta$-methylene interaction from spin density located on $C_\beta$ itself, in accord with previous experimental[49] and theoretical[51] results.

**Unpaired Spin Density at $C_4$, O.** The above analyses show that the unpaired spin density is predominantly delocalized over the phenol ring and oxygen atom. Therefore, the conservation condition, $\sum \rho_i = 1$, for the total unpaired spin density in the $\pi$-system is used to estimate a total unpaired spin density for the combined $C_4$ and O centers of 0.25.

**Estimation of $B_0$ and $B_2$.** The dominant physical origins and value of the $B_0$ term have not been ascertained.[19b,48] Substituting the two measured isotropic couplings and the value of $\rho_\pi = 0.36$ determined from the dipolar coupling into eq 1, and assuming reasonable $B_2$ values[19b,49] for $^2H$ ($^1H$) coupling of 21.5–24.9 MHz (140–162 MHz), we obtain a limit on the value of $B_0$ for the methylene-$^2H$ in the $Y_D$ radical of $<|0.1|$ MHz. The negligible value may arise from the cancellation of oppositely signed spin polarization and direct charge-transfer contributions to the coupling.[48a,b,51] As detailed below, the methylene-$^2H$ in $Y_D^\bullet$ are locked in a discrete conformation. Therefore, if the results obtained here for the tyrosine radical are assumed to be general for $\beta$-hyperfine coupling in neutral radicals, the requirement for a $B_0$-type term in other solid-state systems appears to be linked to dynamic disorder in $\theta$.[52]

Values for $B_2$ for the strong and weak methylene-$^2H$ interactions of 25.7 MHz are obtained by substituting the two isotropic couplings and dipolar-determined $\rho_\pi$ at $C_1$ into eq 2. These $B_2$ values are in good agreement with the value of 24.9 MHz calculated from $A_{iso}$ for freely rotating $\beta$-methyl-$^1H$ in alkyl radicals in solution.[49] In the alkyl radical systems, unit spin density in a pure p-orbital located on $C_\alpha$ and $\langle \cos^2\theta \rangle_{ave} = 0.5$ can be assumed.[49] We therefore conclude that the value of $B_2 = 24.9$ MHz, determined under free rotation in solution,[49] is suitable for analysis of $\beta$-hyperfine interactions in the solid state by use of eq 2. This corroborates the expectation that hyperconjugative $\beta$-hydrogen coupling in neutral radicals should be independent

(49) Fessenden, R. W.; Schuler, R. H. *J. Chem. Phys.* **1963**, *9*, 2147–2195.
(50) Mims, W. B. *Phys. Rev.* **1968**, *168*, 370–381.
(51) Lazdins, D.; Karplus, M. *J. Chem. Phys.* **1966**, *44*, 1600–1611.
(52) (a) Horsfield, A.; Morton, J. R.; Whiffen, D. H. *Mol. Phys.* **1961**, *4*, 425–431. (b) Stone, E. W.; Maki, A. H. *J. Chem. Phys.* **1962**, *37*, 1326–1333. (c) Miyagawa, I.; Itoh, K. *J. Chem. Phys.* **1962**, *36*, 2157–2163.

of whether the p-orbital is involved in $\pi$-conjugation or whether the coupling is directed to protons bonded to primary, secondary, or tertiary carbon.[53,54]

**Limits on the Static and Dynamic Disorder of the $\beta$-$^2H$ Nuclei.** The theoretical model for the $\beta$-hyperfine coupling from which eq 2 is derived is valid for discrete $\theta$ and can thus only be applied validly to a single $C_1$—$C_\beta$ rotamer. Limits on static or dynamic disorder in the $Y_D^\bullet$ $\beta$-methylene interactions can be obtained by considering differential effects of the dispersion on the line widths of the $^2H_{\beta,1}$ and $^2H_{\beta,2}$ $\nu_\alpha$ features. We assume that the $|120°|$ difference between $\theta_1$ and $\theta_2$ is maintained. Static conformational dispersion about a mean $\theta$ value ($\theta_0$) would be manifested in different line widths for the two $\beta$-$^2H$ interactions, because $dA_{iso}/d\theta$ differs for different $\theta_0$. Assuming a detectable line-width difference for the $^2H_{\beta,1}$ and $^2H_{\beta,2}$ $\nu_\alpha$ features of 0.1 MHz leads to an upper limit of $\pm 4°$ on the static dispersion about the $\theta_0$ values of 52° and 68°. Since microwave pulse manipulation of the magnetization in $Y_D^\bullet$ occurs over 0.1–1 $\mu$s depending on $\tau$ value, dynamic disorder caused by fluctuations in $\theta$ that occur on time scales slower than this appears as static disorder and is therefore subject to the limiting $\Delta\theta_0$ estimated above. Fluctuations of $>4°$ about $\theta_0$ occurring on the time scale of application of the microwave pulses would be revealed in differential, $\tau$-dependent line widths. No dependence of the line widths on $\tau$ is observed. For fluctuations in $\theta$ occurring at >10 MHz, calculations based on theoretical descriptions of the dependence of the isotropic coupling on restricted rotation[52b,55] suggest that differential effects on the $^2H$ line shapes would be too small to detect by ESEEM at our experimental signal-to-noise. However, it is unlikely that significant, large-amplitude excursions occur at these frequencies. A locked conformation of the methylene bridge is indicated by the comparable EPR spectra that are observed from room to cryogenic temperatures.[4,15] The EPR spectra are shaped primarily by the strong methylene- and 3,5-$^1H$ hyperfine interactions. Over the narrower temperature range 4.2–77 K, we also observe no change in the ESEEM line widths. The conformation observed in the ESEEM studies at cryogenic temperatures is therefore discrete within the limits of uncertainty of the analysis and appears to reflect the physiological conformation.

**3. Implications for Electron-Transfer Function of $Y_D^\bullet$ and $Y_Z^\bullet$ in Photosystem II.** Comparison of the spin density distributions and dihedral angles among $Y_D^\bullet$ and the model tyrosine neutral radicals allows exploration of channels available for protein influence of the reactivity and thermodynamic stability of tyrosine radicals and to what degree any of these are implemented in PS II.

**Influence of the Methylene Bridge Conformation at $C_1$—$C_\beta$ on $\rho_\pi$ Distribution and Radical Energetics.** The unpaired spin density distribution in $Y_D^\bullet$ is comparable with that in the model tyrosine neutral radicals in the solid state in crystals of L-tyrosine[12] and in vitreous medium.[16,17] In the crystal, the $\theta$ values for the two methylene protons are approximately 30° and 90°, and in the glass a distribution of $\theta$ values of 30–60° and 60–90° is observed,[17] which bracket roughly the values of 52° and 68° in $Y_D^\bullet$. Therefore, the conformation of the methylene bridge does not exercise a significant influence on the distribution of unpaired spin density in the phenol ring of the radical. There is also no detectable unpaired $\pi$ spin density at $C_\beta$ in $Y_D^\bullet$ and thus no resonance stabilization of the radical through significant $p_\pi$–$p_\pi$-orbital coupling with the methylene center. Delocalization of the unpaired spin density in the singly occupied molecular orbital onto the methylene center is, however, afforded by hyperconjugation, as evidenced by the relatively low anisotropy, strong isotropic coupling of the $H_\beta$ nuclei. The absence of significant alteration of the $\pi$ spin densities in the phenol ring among $Y_D^\bullet$ and the model solid-state tyrosine radicals by the hyperconjugation is consistent with the following: (a) the observed transfer of a minute amount of unpaired spin density (<0.02), (b) the comparable hyperconjugation with bonds to $\beta$-hydrogen and $\beta$-carbon,[56,57] and (c) the integrated extent of hyperconjugation, proportional to $\sim 1.5B_2$, is independent of $\theta$ to first order.[57,19b] Therefore, adjustment of the conformation of the methylene bridge does not appear to be a likely mechanism for protein control of the unpaired spin density distribution in and, hence, the electronic energy of, $Y_D^\bullet$ or catalytic tyrosine radicals in other enzymes.

Hyperconjugation in closed-shell systems, such as diamagnetic tyrosine, is far less favorable energetically than in $\pi$-electron-deficient radical or cationic systems.[54,56,58] In corroboration of this, there is no evidence for shortening of the $C_1$—$C_\beta$ single bond owing to hyperconjugation in diamagnetic tyrosine in the crystal (1.51 Å)[47] beyond that expected for a C—C $\sigma$-bond formed from $sp^2$–$sp^3$ hybrid orbitals.[53] Therefore, strong hyperconjugation between the ring and the $C_\beta$ center is a unique feature of the radical state. The selective lowering of energy of the tyrosine radical species by the hyperconjugation would contribute favorably to ease of oxidation of $Y_D$ to $Y_D^\bullet$. On the basis of the influence of methyl-group substitution on the first ionization potentials of several charge-neutral aromatic ring systems,[53] the contribution of hyperconjugation could lower the potential for oxidation of tyrosine by up to 0.2 eV.

The lack of detectable unpaired $\pi$ spin density at $C_\beta$ suggests that the bond order of the $C_1$—$C_\beta$ bond in the radical is not perturbed significantly from that of the $C_1$—$C_\beta$ single bond in diamagnetic tyrosine.[12,47] This suggests that the $\theta$-dependence and maximum height ($V_0$) of the $C_1$—$C_\beta$ bond internal torsion potential energy are comparable in the radical and in diamagnetic tyrosine. Hyperconjugation in the radical makes a negligible contribution (estimated crudely at $\approx$0.3 kcal/mol)[53] to the torsion potential barrier in C—C single bonds. A comparable torsion potential profile for radical and diamagnetic states is also supported by the absence of substantial distortion of the tyrosine radical conformation in single crystals of L-tyrosine relative to that of the diamagnetic tyrosine present prior to irradiation.[12] Therefore, static or dynamic protein control of the $C_1$—$C_\beta$ torsion potential energy does not appear to be a significant mechanism for influencing the redox potential through differential stabilization of the diamagnetic and radical tyrosine.

**Influence of Delocalized Solvation Interactions with the Protein on $\rho_\pi$ Distribution.** The solvating environments of $Y_D^\bullet$ and the model radicals differ distinctly. $Y_D$ is located deep within the protein[59,60] in a region predicted to be apolar.[61] This environment differs distinctly from that in the crystal, which presents an ordered array of electrostatic charges, and the bulk charge distribution in the high-dielectric, aqueous glass media. Despite these different environments, the unpaired spin density distributions in $Y_D^\bullet$ and in the solid-state model radicals are comparable. Therefore, the dielectric properties of the medium exert little influence on the distribution of unpaired spin density and, hence, the energy of the singly occupied molecular orbital, in the tyrosine radicals.

**Influence of Localized Electrostatic Interactions at the Phenol Oxygen Atom on $\rho_\pi$ Distribution.** Our results show that neither the methylene bridge conformation nor delocalized solvent interactions influence significantly the distribution of $\rho_\pi$ in the tyrosine radicals. However, hydrogen bonding or other localized electrostatic interactions at the phenol oxygen atom may have the capacity to perturb the $\rho_\pi$ distribution. This is suggested by apparent differences between the $\rho_\pi$ distribution in $Y_D^\bullet$, which

(53) Coulson, C. A. *Valence*; Oxford University Press: New York, 1961; pp 356–369.
(54) Dewar, M. J. S. *Hyperconjugation*; Ronald Press: New York, 1962.
(55) Bauld, N. L.; McDermed, J. D.; Hudson, C. E.; Rim, Y. S.; Zoeller, J., Jr.; Gordon, R. D.; Hyde, J. S. *J. Am. Chem. Soc.* **1969**, *91*, 6666–6676.
(56) Mulliken, R. S. *Tetrahedron* **1959**, *5*, 253–274.
(57) Stock, L. M.; Suzuki, J. *J. Am. Chem. Soc.* **1965**, *87*, 3909–3913.
(58) Symons, M. C. R. *Tetrahedron* **1962**, *18*, 333–341.
(59) Rodriguez, I. D.; Chandrashekar, T. K.; Babcock, G. T. In *Progress in Photosynthesis Research*; Biggins, J., Ed.; Nijhoff: Dordrecht, 1987; Vol. 1, pp 471–474.
(60) Innes, J. B.; Brudvig, G. W. *Biochemistry* **1989**, *28*, 1116–1125.
(61) Svensson, B.; Vass, I.; Cedergren, E.; Styrring, S. *EMBO J.* **1990**, *9*, 2051–2059.

forms a hydrogen bond with protein[9,11,59,62] (Espe, M.; Babcock, G. T. Unpublished) and the non-hydrogen-bonded tyrosine radical of ribonucleotide diphosphate reductase,[21] and hydrogen-bonding interactions on $\rho_O$ in semiquinones.[63] We are engaged in studies that address the influence of hydrogen bonding on $\rho_\pi$ distribution in tyrosine radicals and will report the results in a subsequent publication.

**Influence of the Methylene Bridge on Electron-Transfer Rates: Donor–Acceptor Electronic Coupling.** In the oxidized radical state of tyrosine, hyperconjugation extends spatially the $\pi$-electron distribution associated with the highest energy, singly occupied orbital by approximately 1.5 Å along the direction of the $C_1$—$C_\beta$ bond, relative to the diamagnetic state of tyrosine. The rates of long-range, nonadiabatic electron-transfer reactions between redox centers in proteins depend sensitively on the distance-dependent overlap of the donor (D) and acceptor (A) electronic wave functions.[64,65] The separation distance, $r$, between $\pi$-conjugated organic donors and acceptors is measured conventionally from the shortest distance between the centers of the atoms on the perimeter of the $\pi$-electron distribution, plus a van der Waals contact term, $r_0$ = 3.0–3.6 Å.[64a] Therefore, on the basis of an exponential decay parameter, $\beta$, of 1.4 Å$^{-1}$ for electronic coupling through protein,[66] the hyperconjugative extension yields a maximum enhancement in rate of ~12-fold when the $C_1$—$C_\beta$ bond lies along the direction of the electron-transfer partner, relative to the absence of the hyperconjugation.

Figure 6 depicts a model for the enhancement of directional selectivity in electron transfer from a donor (D) to acceptor (A) through an intermediate (I) that is achievable, in principle, from the redox state-dependent hyperconjugation in I.[65] The electronic coupling between the D and I redox sites is enhanced in the state $DI^{\bullet+}A$ relative to $D^{\bullet+}IA$; that is, $r_{DI} < r_{DI'}$, in proportion to the projection of the vector describing the hyperconjugative extension onto the intersite vector. The condition $r_{DI} < r_{DI'}$ leads to enhancement of the rate of the desired electron transfer from D to $I^{\bullet+}$ and a relative attenuation of the undesired recombination reaction that reforms $D^{\bullet+}$ from I. For short electron transfers (<5 Å), covalent grafting of the cofactor to the polypeptide would also circumvent the proposed[67] rate-diminishing through-space jumps or through-hydrogen-bond transmission required in the case of dissociable cofactors and thus increase the reaction rate. However, this would not appear to be important for the longer range (>10 Å) physiological electron-transfer reactions[6] mediated by $Y_D^\bullet/Y_D$ and $Y_Z^\bullet/Y_Z$ in the PS II RC protein.[66]

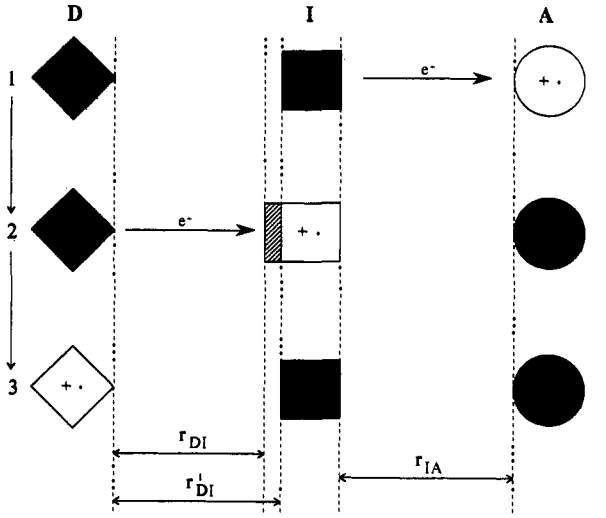


**Figure 6.** Depiction of an electronic mechanism for enhanced directional selectivity in electron transfers involving an intermediate redox site. Progress from state 1 to state 3 can be viewed as movement of the "transferred electron" [64c] from donor (D) to acceptor (A) through the intermediate redox site (I), or of hole transfer from A to D through I. Oxidation of I by the oxidized acceptor site ($A^{\bullet+}$) promotes hyperconjugative extension of the highest energy molecular orbital containing the unpaired electron, represented as the cross-hatched area on $I^{\bullet+}$ in state 2. Re-reduction of $I^{\bullet+}$ by D collapses the hyperconjugative extension. Changes in the value of the electron-transfer matrix element, caused by changes in the separation of the D and I sites owing to hyperconjugation, are depicted by the lengths of the double-ended arrows. A decrease in $T_{DI,0}$ versus $T_{DI,0'}$ can also account for enhanced coupling in this case of a single D-I-A system equilibrium nuclear geometry.[65]

If the hyperconjugative extension mechanism is operative in the PS II RC protein, D, I, and A in Figure 6 could represent the manganese center, tyrosine, and primary donor, respectively. The small free energies for the rapid electron-transfer reactions mediated by $Y_Z^\bullet/Y_Z$[6] indicate that directed hyperconjugation and discrete positioning of the phenol ring by the protein are central in satisfying the requirements for optimal dual $Y_Z$ donor, $Y_Z^\bullet$ acceptor function in shuttling electrons between the manganese center and the primary donor.

**Acknowledgment.** We thank Dr. Matthew Espe, Dr. Neil Bowlby, Matthew Gardner, and Rita Bhatnagar, for preparation and provision of PS II samples from *Synechocystis*, and Professors Dan Nocera and Jim Harrison for helpful discussions.

(62) Mino, H.; Satoh, J.; Kawamori, A.; Toriyama, K.; Zimmerman, J.-L. *Biochim. Biophys. Acta* **1993**, *1144*, 426–433.

(63) (a) Gulick, W. M.; Geske, D. H. *J. Am. Chem. Soc.* **1966**, *88*, 4119–4124. (b) Feher, G.; Isaacson, R. A.; Okamura, M. Y.; Lubitz, W. In *Antennas and Pigments of Photosynthetic Bacteria*; Michel-Beyerle, M. E., Ed.; Springer-Verlag: Berlin, 1985; pp 174–189. (c) Reiter, R. C.; Stevenson, G. R.; Wang, Z. Y. *J. Phys. Chem.* **1990**, *94*, 5717–5720.

(64) (a) Marcus, R. A.; Sutin, N. *Biochim. Biophys. Acta* **1985**, *811*, 265–322. (b) DeVault, D. *Quantum Mechanical Tunnelling in Biological Systems*; Cambridge University Press: New York, 1984. (c) Newton, M. D. *Chem. Rev.* **1991**, *91*, 767–792. (d) Evenson, J. W.; Karplus, M. *J. Chem. Phys.* **1992**, *96*, 5272–5278.

(65) The rate constant for nonadiabatic electron transfer is proportional to the square of the electron-transfer matrix element, $T_{ij}$, where $i$ and $j$ represent donor and acceptor redox sites. The matrix element has been expressed commonly in the simple form $T_{ij,0}\exp[-(\beta(r-r_0)/2]$,[64a-c] which describes well the experimental rate–distance dependence of many biological, nonadiabatic electron-transfer reactions.[66] The value of $T_{ij,0}$ gives the electronic coupling at van der Waals contact, and the degree of decay of the electronic coupling for $r > r_0$ is determined by the attenuation factor, $\beta$. The hyperconjugation-enhanced electronic coupling can be described in terms of parameters included in the empirical, exponential-decay expression as an increase in $T_{DA,0}$ or as a decrease in $\beta$ or $r$. Here, changes in $r$ are chosen to convey changes in $T_{ij}$. A detailed analysis of this model will be presented in a later report.

(66) Moser, C. C.; Keske, J. M.; Warncke, K.; Farid, R. S.; Dutton, P. L. *Nature* **1992**, *355*, 796–802.

(67) (a) Beratan, D. N.; Betts, J. N.; Onuchic, J. N. *Science* **1991**, *252*, 1285–1288. (b) Onuchic, J. N.; Beratan, D. N.; Winkler, J. R.; Gray, H. B. *Annu. Rev. Biomol. Struct.* **1992**, *21*, 349–377.